Molecular Therapy
Nucleic Acids
Original Article

siRNA-Encapsulated Hybrid Nanoparticles Target Mutant K-*ras* and Inhibit Metastatic Tumor Burden in a Mouse Model of Lung Cancer

Maryna Perepelyuk,[1] Olubunmi Shoyele,[2] Ruth Birbe,[3] Chellappagounder Thangavel,[4] Yi Liu,[4] Robert B. Den,[4] Adam E. Snook,[5] Bo Lu,[4] and Sunday A. Shoyele[1]

[1]Department of Pharmaceutical Science, College of Pharmacy, Thomas Jefferson University, Philadelphia, PA 19107, USA; [2]Department of Pathology and Laboratory Medicine, Western Connecticut Health Network, Danbury Hospital, Danbury, CT 06810, USA; [3]Department of Pathology and Laboratory Medicine, Cooper University Hospital-MD Anderson Cancer Center, Camden, NJ 08103, USA; [4]Department of Radiation Oncology, Thomas Jefferson University, Philadelphia, PA 19107, USA; [5]Department of Pharmacology and Experimental Therapeutics, Thomas Jefferson University, Philadelphia 19107, PA, USA

There is an unmet need in the development of an effective therapy for mutant K-*ras*-expressing non-small-cell lung cancer (NSCLC). Although various small molecules have been evaluated, an effective therapy remains a dream. siRNAs have the potential to downregulate mutant K-*ras* both at the protein and mRNA levels. However, a safe and effective delivery of siRNAs to tumors remains a limitation to their translational application in the treatment of this highly debilitating disease. Here we developed a novel hybrid nanoparticle carrier for effective delivery of anti-mutant K-*ras* to NSCLC (AKSLHN). The ability of this treatment modality to regress lung tumors in mouse models was evaluated as a monotherapy or as a combination treatment with erlotinib. Further, the toxicity of this treatment modality to healthy tissues was evaluated, along with its ability to elicit immune/inflammatory reactions. The results suggest that this treatment modality is a promising prospect for the treatment of mutant K-*ras*-expressing NSCLC without any accompanying toxicity. However, further understanding of the cellular-level interaction between AHSLHN and erlotinib needs to be attained before this promising treatment modality can be brought to the bedside.

INTRODUCTION

Non-small cell lung cancer (NSCLC) is the leading cause of cancer mortality in the United States and the world, with a 5-year survival rate of only 15% for all stages combined, despite some recent advances in chemotherapeutic agents.[1,2] The size and distribution of NSCLC makes cytoreductive surgery ineffective.[3] Consequently, chemotherapy and/or radiation have been the treatments of choice. Conventional chemotherapy regimens have had limited efficacy, mainly because of resistance of these cancer cells to chemotherapeutic agents.[4,5] Small-molecule inhibitors such as erlotinib and afatinib that target the tyrosine kinase domain of epidermal growth factor receptor (EGFR) produce responses in approximately 10% of patients with NSCLC.[6–8] In patients with mutant EGFR, responses to EGFR-tyrosine kinase inhibitors (EGFR-TKIs) can be dramatic and may last longer than a year. In contrast, K-*ras* gene mutation, which occurs in approximately 30% of NSCLC, has been associated with a poor response to EGFR-TKIs.[9–13] It has been demonstrated previously that somatic mutations in the tyrosine kinase domain of EGFR are associated with sensitivity to EGFR-TKIs,[14] whereas mutations in K-*ras*, which encodes a guanosine triphosphotase (GTPase) downstream of EGFR, are associated with primary resistance.[9] Thus, mutant K-*ras* inhibition may be critical for successful NSCLC treatment. However, there is an unmet need in developing the most appropriate therapy for mutant K-*ras* NSCLC. Several strategies, such as farnesyltransferase inhibitors, have been explored as possible inhibitors of mutant K-*ras* in lung adenocarcinomas. To date, none of these strategies have proved to be successful, mainly because of lack of specificity. Often, undesirable inhibition of wild-type K-*ras* is also achieved. Small interfering RNA (siRNA) inhibition is a very viable alternative given the specificity of this technology. Here we aim to harness the advantages of siRNA technology as a therapeutic modality for mutant K-*ras* in NSCLC. siRNA as a therapeutic molecule is very effective at knocking down molecular pathways that are pathogenic.[15] However, its application in the clinic is often limited by its susceptibility to enzymatic degradation in blood, non-specific uptake by cells, and the difficulty involved in the transfection of siRNA to cells because of its relatively large size and polarity.[16,17]. Clearance by the mononuclear phagocyte system (MPS) is another limiting factor affecting the possible therapeutic application of siRNA.[18–20] Recently, our group developed a novel hybrid nanoparticle delivery system composed of human immunoglobulin G (IgG) and poloxamer-188 (a polyoxyethylene-polyoxypropylene block copolymer) for stable and efficient siRNA delivery to lung adenocarcinoma cells.[21–23] We hypothesized that our hybrid nanoparticles would efficiently deliver loaded anti-mutant K-*ras* siRNA into the cytosol of

Received 25 August 2016; accepted 9 December 2016;
http://dx.doi.org/10.1016/j.omtn.2016.12.009.

Correspondence: Sunday A. Shoyele, Department of Pharmaceutical Sciences, School of Pharmacy, Thomas Jefferson University, 901 Walnut Street, Philadelphia, PA 19107, USA.
E-mail: sunday.shoyele@jefferson.edu

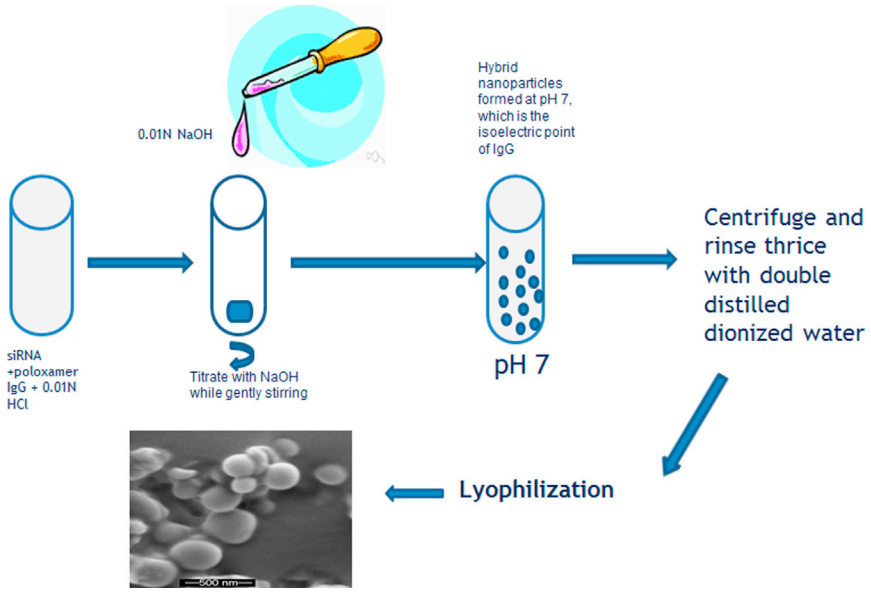

Figure 1. Preparation of AKSLHNs
The schematic shows the development of AKSLHNs based on the precipitation of IgG at its isoelectric point.

lung adenocarcinoma cells, downregulate G12S-K-*ras* in A549 cells, and inhibit cancer cell proliferation. Further, in view of the fact that human IgG is the main immunoglobulin that protects the body against infection, we hypothesized that these hybrid nanoparticles would not produce the well documented immunogenic/inflammatory reaction experienced with most nanoparticle formulations. Poloxamer- 188, a nonionic triblock copolymer, is added to the surface of the nanoparticles to help circumvent the MPS during systemic circulation.[21] Data obtained in vitro in cell culture supported these hypotheses and demonstrated the effectiveness of these hybrid nanoparticles in accomplishing the set objectives.[21,23] An anti-proliferation effect of anti-mutant K-*ras* siRNA-loaded hybrid nanoparticles (AKSLHNs) in A549 cells was also demonstrated.[21,22] Further, our findings demonstrated that the double-layer protection provided by these nanoparticles helps to protect enclosed siRNA from serum nucleases for up to a minimum of 48 hr.

The main objective of the present study was to validate the results obtained from in vitro studies under in vivo conditions using a metastatic orthotopic murine model of NSCLC. To achieve this, we hypothesize that AKSLHNs will inhibit the progression of metastatic lung cancer by efficiently downregulating mutant-K-*ras* in mouse models without eliciting an immune/inflammatory reaction. Further, we hypothesize that AKSLHNs will not cause unnecessary toxicity to normal tissues because of their preferential accumulation in tumors compared with normal tissues. This is based on the fact that tumors are naturally more permeable to particles between 100–800 nm because of an enhanced permeation and retention (EPR) effect.[24]

To test these hypotheses, metastatic orthotopic murine models of NSCLC were created by injecting A549-luc cells into the tail veins of female severe combined immunodeficiency (SCID) beige mice. The tumor burden was monitored using Xenogen IVIS bioluminescence imaging. The efficacy of intraperitoneally injected AKSLHNs at inhibiting or downregulating mutant K-*ras* and slowing down tumor progression was compared with several control formulations.

RESULTS

Nanoparticle Formation and Characterization

AKSLHNs composed of human IgG in the inner layer and poloxamer-188 in the outer layer were prepared using our previously reported nanoprecipitation process.[21–23] Figure 1 shows a schematic of AKSLHN development. AKSLHNs were spontaneously produced at pH 7.0, which is the isoelectric point of human IgG. Photon correlation spectroscopy (PCS) demonstrated that these particles were 135.4 ± 5.4 nm in diameter, with a polydispersity index (PI) of 0.07 ± 0.03. These particles demonstrated a zeta potential of +16.7 ± 0.2 and encapsulation efficiency and loading efficiency of 60% ± 0.4% and 2.04% ± 0.06%, respectively.

Maximum Tolerated Dose Determination

The maximum tolerated dose (MTD) of siG12S in AKSLHNs was determined for in vivo experiments by administering different doses of AKSLHNs (0.1, 0.3, 0.6, 0.9, and 1.2 mg/kg body weight equivalent of siG12S) progressively by intraperitoneal injection to female nu/nu nude mice. 24 hr after the last dose was injected, the animals were euthanized, and their kidneys, lungs, and livers were harvested. The tissues from these organs were evaluated for apoptosis using cell death detection ELISA. The results demonstrated that the AKSLHNs had no effect on animal mortality, behavior, or body weight up to 0.9 mg/kg body weight. Apoptosis evaluation demonstrated that the nanoparticle formulation did not cause any significant damage to the liver, lung, and kidney compared with the untreated control up to 0.9 mg/kg (Figure 2).

Antitumor Effect of AKSLHN in Metastatic Orthotopic Murine NSCLC Models

The tumor burden in mice was monitored using the Xenogen IVIS bioluminescence imaging system. Mice treated with AKSLHNs showed regression in tumor burden over the 4-week experimental period. In contrast, PBS-treated control, erlotinib-treated, and combination-treated (AKSLHNs and erlotinib) groups showed lack of sensitivity to their respective treatment, as demonstrated by tumor progression (Figure 3). The tumor burden was quantified by measuring the photon counts for each tumor, which was then plotted against time (weeks) to further demonstrate the antitumor effect of

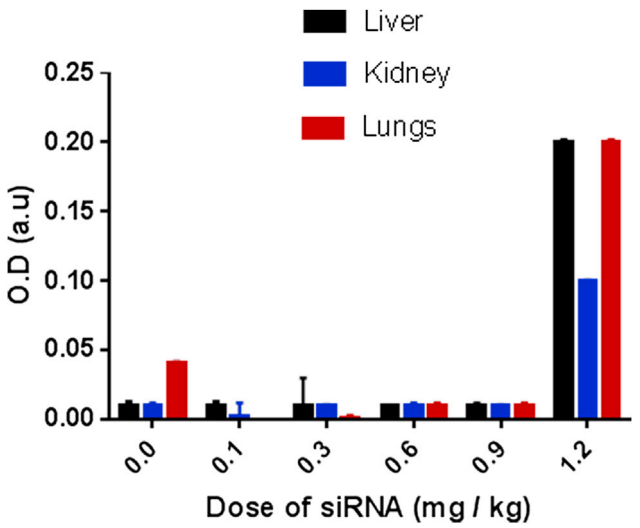

Figure 2. Determination of the Maximum Tolerable Dose in Female nu/nu Nude Mice

No apoptosis was observed in the livers, kidneys, and lungs of the mice up to 0.9 mg/kg dose of anti-mutant K-*ras* siRNA in AKSLHNs (n = 3).

injected AKSLHNs, as shown in Figure 4A. The tumor burden in PBS-treated mice continued to progress until metastasis in the colorectal area was observed after 2 weeks of treatment. Metastasis of tumors to both the left and right lumber lymph nodes[25] and the colorectal region could also be conspicuously observed after 3 weeks of monitoring. We also observed metastasis to the right or left popliteal lymph nodes in some of the mice (Figure S1). To confirm metastasis to other organs, the lungs, heart, liver, and kidneys of PBS-treated mice were harvested after the mice were euthanized and imaged ex vivo using Xenogen IVIS bioluminescence. Metastasis to the liver and heart was demonstrated in these mice, as shown in Figure S2. Similarly, the erlotinib-treated and combination-treated groups demonstrated evidence of metastasis to the colorectal region of the mice. Interestingly, tumor metastasis to the brain was observed in one of the five mice in the erlotinib-treated group after 3 weeks of treatment (Figure S2). This mouse died 1 day after imaging.

Apoptosis determination by cell death ELISA and TUNEL showed that AKSLHNs enhanced apoptosis induction in lungs with tumors (Figures 4B and 4C).

In contrast, erlotinib-, combination-, and PBS-treated lungs with tumors only demonstrated limited evidence of apoptosis.

Downregulation of Targeted mRNA and Proteins

Expression of mutant K-*ras* G12S mRNA was studied in the tumors using TaqMan qRT-PCR and western blot analysis (Figures 5A and 5B). The western blot data in Figure 5A demonstrate that AKSLHNs downregulated mutant K-*ras* compared with PBS, combination, and erlotinib. qRT-PCR showed that AKSLHNs significantly downregulated mutant K-*ras* mRNA by approximately 60% compared with PBS. Further, combination and erlotinib treatments did not show any effect on mutant K-*ras* expression, as shown in Figure 5B.

Adenocarcinoma Histology

Adenocarcinoma of mice treated with AKSLHNs showed smaller tumors with thin fibrovascular stroma and rare mitotic figures (Figure 6A). Mice that received a combination of erlotinib and AKSLHNs showed few mitotic figures on H&E, as shown in Figure 6B.

Adenocarcinomas from mice treated with erlotinib had numerous mitotic figures (Figure 6C). The tumor cells had foamy vacuolated cytoplasm, eccentric nuclei, and prominent nucleoli. There was lymphovascular invasion. Mice from the control group (PBS) had multinucleated tumor cells with eosinophilic cytoplasm, as shown in Figure 6D. There was lymphovascular invasion with a high mitotic rate.

Toxicity to Normal Tissues

Toxicity to healthy tissues was evaluated using cell death detection ELISA to detect the induction of apoptosis. Figure 7A demonstrates that AKSLHNs did not lead to apoptosis in the lung, kidney, and liver of treated animals after 4 weeks of treatment. This is similar to the untreated control. Similarly, the combination-treated group did not show any apoptosis in any of these critical organs. However, the erlotinib-treated group showed signs of apoptosis in the liver, as demonstrated in Figure 7A.

Inflammatory/Immunogenic Reaction

Cytokines interleukin-6 (IL-6) and tumor necrosis factor α (TNF-α) levels were measured in both cultured splenocytes isolated from spleens harvested from treated mice and serum using the respective ELISA kits. Figure 7B shows that AKSLHNs did not significantly increase IL-6 expression in the spleens of treated mice compared with PBS except for day 2 post-treatment. Similarly, TNF-α did not significantly increase in the splenocytes of treated mice throughout the 8-day study period.

Expression of both IL-6 and TNF-α in the sera of treated mice was also evaluated. Figure S3 shows that there was no significant increase in the levels of both IL-6 and TNF-α throughout the period of study.

DISCUSSION

AKSLHNs were specially designed to facilitate the delivery of anti-mutant K-*ras* siRNA to mutant K-*ras*-expressing metastatic lung cancer in an orthotopic mouse model. It was hypothesized that AKSLHNs will inhibit the progression of metastatic lung cancer by efficiently downregulating mutant-K-*ras* in mouse models without eliciting immune/inflammatory reactions. Further, we hypothesized that AKSLHNs will not cause unnecessary toxicity to normal tissues because of their preferential accumulation in tumors compared with normal tissues. It has been reported that an unmet need still exists in finding an appropriate therapy for mutant K-*ras*-expressing lung cancer because various treatment modalities, including farnesyltransferase inhibitors, have yet to yield positive results.[9] However, siRNAs are known to have the potential to silence critical molecular pathways

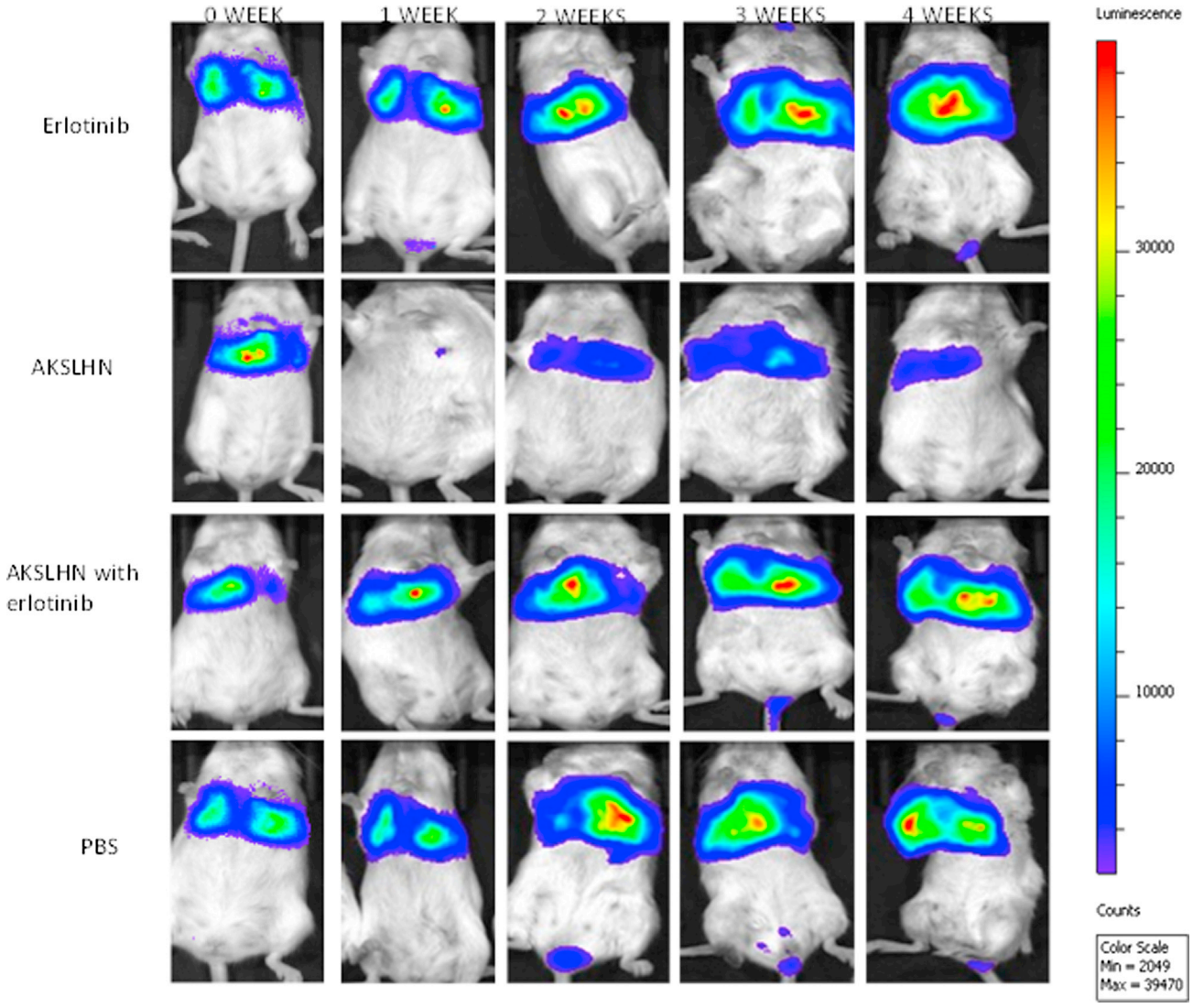

Figure 3. Antitumor Effect of AKSLHNs in Comparison with Various Controls

AKSLHNs inhibited tumor progression following intraperitoneal administration of 0.3 mg/kg siRNA content into SCID beige mice.

responsible for pathogenic conditions. The use of siRNA as a therapeutic tool is, however, being compromised by a lack of safe and efficient delivery systems, limiting the efficacy of these molecules in the clinic. In this study, AKSLHNs are being evaluated as a potential treatment modality in mutant K-*ras*-expressing metastatic lung cancer. AKSLHNs were prepared based on the fact that proteins have minimum solubility but maximum precipitation at the isoelectric point.[21,22] AKSLHNs were very effective in regressing lung tumors in mice, as shown in Figure 3, after 4 weeks of treatment. In contrast, such potency was not observed when AKSLHNs were combined with erlotinib. A combination of AKSLHNs and erlotinib was evaluated under the hypothesis that the downregulation of mutant K-*ras* by AKSLHNs would improve the sensitivity of mutant K-*ras*-expressing lung cancer to EGFR-TKIs because mutant K-*ras* has been implicated in the lack of efficacy of EGFR-TKIs in lung cancer with mutant K-*ras* expression.[9,14,26,27] Surprisingly, this combination treatment produced an inferior antitumor effect compared with AKSLHNs alone. This suggests an unfavorable interaction between the concurrently administered AKSLHNs and erlotinib. We previously reported that our hybrid nanoparticles are able to escape endocytic recycling and are successfully delivered to the cytosol of target cells because of the buffering capacity of the hybrid nanoparticles in the endosome. The solubility of IgG and poloxamer-188 at acidic pH levels makes it possible for the dissolved IgG in the endosome to activate the proton pump that raises osmotic pressure in the endosome, leading to the swelling and subsequent escape of siRNA from endosomes into the cytosol.[21,27,28] However, the presence of erlotinib, a very basic drug, in the endosome at the same time may increase the pH level of the

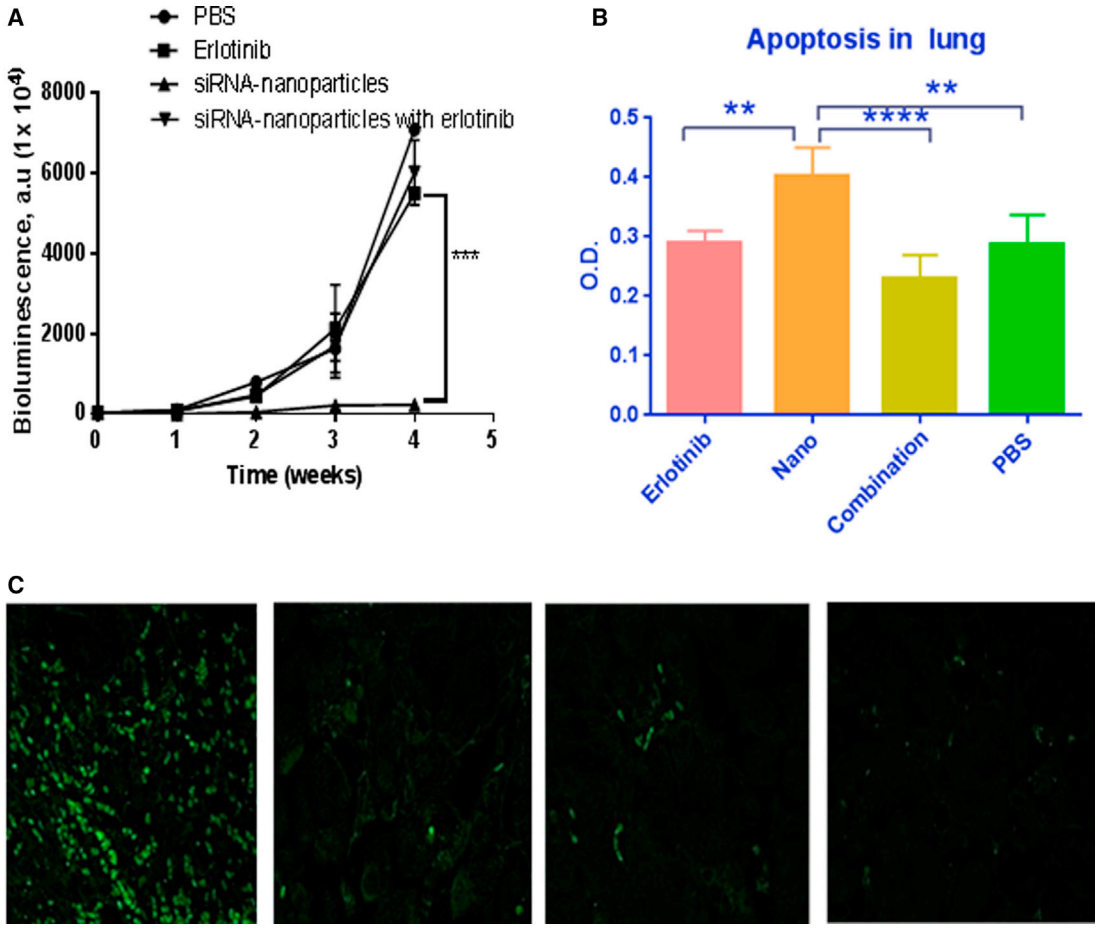

Figure 4. Effect of AKSLHNs on Lung Tumor Inhibition

(A) In vivo evaluation of siRNA nanoparticles in lung tumor-bearing SCID beige mice. IVIS bioluminescence was used for imaging. ***$p \leq 0.001$, n = 3. Error bars are ± SD. (B) Determination of apoptosis in lung tumors using cell death detection ELISA after various treatments in SCID beige mice models. Nano represents AKSLHNs, whereas combination represents AKSLHNs in combination with erlotinib. **$p \leq 0.01$; ****$p \leq 0.0001$ (n = 3). Error bars are ± SD. (C) TUNEL analysis of apoptosis in lung tissue sections from variously treated groups; from left to right: AKSLHNs, erlotinib, combination of AKSLHNs and erlotinib, and PBS treatment.

endosome, making it impossible for the nanoparticles to dissolve and release the siRNA as it would normally do. The lack of release of siRNA because of the presence of erlotinib is assumed to subsequently lead to an inferior antitumor effect of the combination therapy compared with AKSLHNs alone. The interaction between a pH-sensitive nucleic acid-loaded nanoparticle system and a concurrently administered basic drug needs to be investigated further for a clear understanding of this phenomenon. Nevertheless, metastasis of the tumor to the brain, colorectal region, right and left lumber lymph nodes, and right popliteal lymph nodes[24] was observed in the other groups of animals, except the AKSLHN-treated group. The effective antitumor effect of AKSLHNs was further validated by induction of apoptosis in the tumor-bearing lungs of the AKSLHN-treated group using both TUNEL and cell death detection ELISA. Further, both mutant K-*ras* protein and mRNA were significantly downregulated in the lungs of AKSLHN-treated mice compared with the other mouse groups, further validating the effectiveness of this therapy. Previously, we reported the superior and stable downregulation of mutant K-*ras* by AKSLHNs at the cellular level (using A549 cells) over both scramble siRNA and Lipofectamine-delivered anti-K-*ras* siRNA.[21,29]

Toxicity and inflammatory reaction remain the limiting factors preventing the translational application of most nanomedicines.[22,23,30] For any nanoparticle-based therapeutic agent to have a chance of progressing to the clinic, it is important that it is not toxic to healthy tissues and does not elicit a significant immunogenic/inflammatory reaction. On that note, we evaluated the effect of AKSLHNs, erlotinib, and a combination of both on the induction of apoptosis in healthy tissues. Induction of apoptosis in healthy tissues has been reported previously to represent toxicity in such tissues.[4] AKSLHNs and the combination treatment did not lead to induction of apoptosis in the lung, kidney, and liver of treated mice. However, erlotinib as a lone therapy showed some toxicity to the liver. This is not surprising

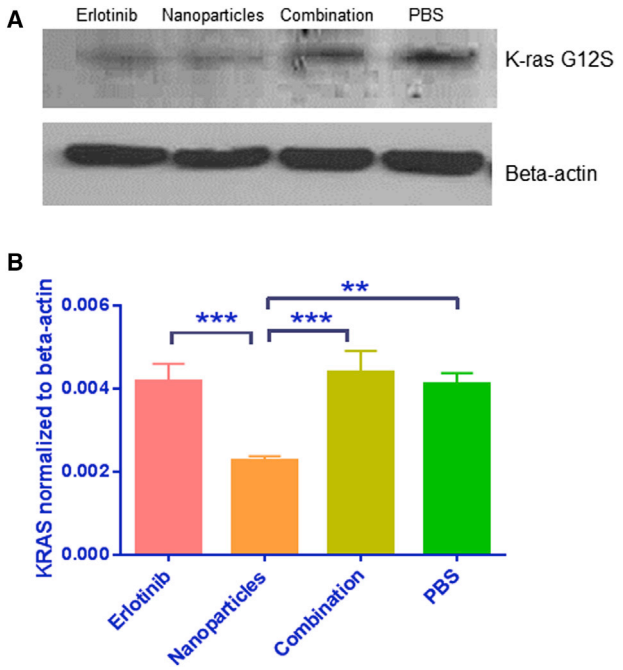

Figure 5. AKSLHNs Enhance In Vivo Downregulation of K-*ras* G12S mRNA and Protein

(A) Western blot analysis shows an enhanced downregulation of target protein (K-*ras* mRNA) by AKSLHNs (nanoparticles) in comparison with PBS and combination treatment. Erlotinib-treated lung tumors also show some downregulation. (B) TaqMan qRT-PCR shows that AKSHLNs (nanoparticles) downregulated K-*ras* mRNA by approximately 50% in comparison with PBS. n = 3; $^{**}p \leq 0.01$; $^{***}p \leq 0.001$. Error bars are ± SD.

because erlotinib has been implicated previously in acute hepatotoxicity in NSCLC patients.[31] It is, however, interesting to note that the combination therapy involving both AKSLHNs and erlotinib did not lead to hepatotoxicity. This further corroborates our hypothesis that an interaction occurs between AKSLHNs and erlotinib at the cellular level. To evaluate the ability of AKSLHNs to elicit an immune/inflammatory response, naive BALB/c mice were used. SCID beige mice used for development of the metastatic orthotopic murine NSCLC model are immunocompromised and would not be suitable for the immunogenic/inflammatory reaction experiment. SCID mice are characterized by the complete inability of the adaptive immune system to mount, coordinate, and sustain an appropriate immune response, usually because of absent or atypical T and B lymphocytes. IL-6 and TNF-α expression in isolated splenocytes and sera of AKSLHN-treated mice was similar to that of PBS-treated (control) mice, except for a certain time point where insignificant elevated expression of these cytokines was observed. This could be attributed to two factors: the presence of poloxamer-188 on the surface of the nanoparticles or the fact that the nanoparticles were fabricated with human IgG and tested in mice. This interspecies variation could contribute to the slight elevation in these cytokines at these time points. Future study will involve the use of mouse IgG in the fabrication of the nanoparticles to eliminate interspecies variation as a contributory factor to this observation.

In conclusion, AKSLHNs are a promising prospect as a treatment modality for mutant K-*ras*-expressing NSCLC as a single therapy. A further understanding of the cellular-level interaction between AKSLHNs and EGFR-TKIs during concurrent administration would help in developing an optimal dosage regimen to further harness this treatment modality in NSCLC patients.

MATERIALS AND METHODS

Human IgG was purchased from Equitech Bio. Poloxamer-188, RNase-free water, and fetal bovine serum were obtained from Fisher Scientific. siRNA against mutated K-*ras* G12S was designed by and purchased from Thermo Scientific (formerly Dharmacon). The siG12S sense and antisense sequences were GUUGGAGCUA GUGGCGUAGdTdT and CUACGCCACUAGCUCCAACdTdT, respectively. Erlotinib hydrochloride was purchased from Fisher Scientific. XenoLight RediJect D-Luciferin Bioluminescent Substrate was obtained from PerkinElmer. Monoclonal antibodies specific for mutant G12S K-*ras* proteins was obtained from NewEast Biosciences. The TNF-α ELISA kit was obtained from Thermo Scientific, and the IL-6 ELISA kit was obtained from Becton Dickinson.

Cell Culture

Human adenocarcinoma cell line A549-luciferase, expressing a K-*ras* mutation at G12S, was obtained from PerkinElmer. These cells were maintained in 10% fetal bovine serum and 1% antibiotics-supplemented F12K. They were kept in a humidified atmosphere with 5% carbon dioxide.

Animals

Female SCID beige mice, 7–8 weeks old and weighing approximately 28 g, and female BALB/c mice were supplied by Taconic and maintained in the American Association for the Accreditation of Laboratory Animal Care (AAALAC)-accredited facility at Thomas Jefferson University. All animal studies were approved by the Institutional Animal Care and Use Committee (IACUC) of Thomas Jefferson University.

Preparation of AKSLHNs

50 mg of excipient-free human IgG was dissolved in 0.01 N HCl containing 20 mg of poloxamer-188. 187 μg of siRNA was then added to make a 10-mL total solution in a 50-mL beaker. The final concentration of human IgG in the solution amounted to 5 mg/mL. This solution was then slowly titrated with 0.01 N NaOH to bring the pH of the mixture to 7, which is the isoelectric point (pI) of human IgG as determined in our laboratory using isoelectric focusing. The nanoparticles were continuously stirred on a magnetic stirrer for 10 min. To isolate the nanoparticles from the precipitation medium, the suspension was centrifuged with a microcentrifuge (Eppendorf centrifuge 5418) at 2,000 rpm for 5 min. Nanoparticles were then rinsed with double-distilled deionized water before being redispersed in water and snap-frozen using liquid nitrogen. This was then loaded into a freeze

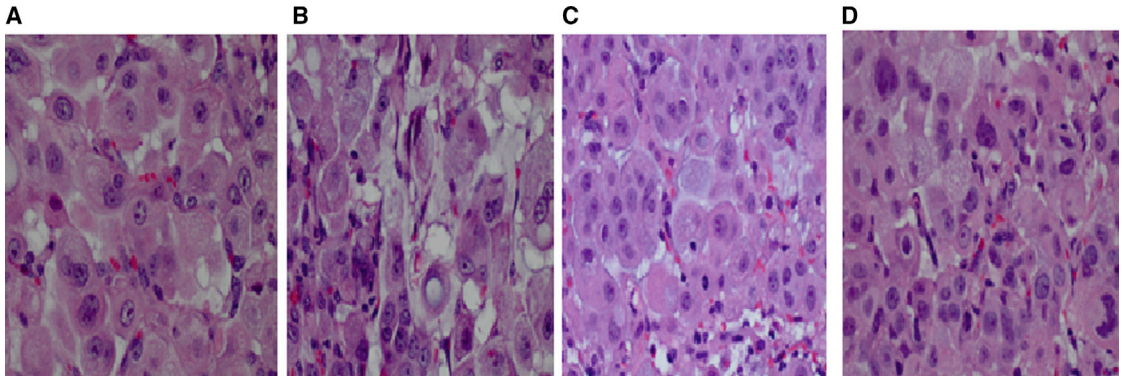

Figure 6. Lung Adenocarcinoma Histopathology
(A–D) H&E-stained slides at 400× magnification. Shown are (A) AKSLHN-treated, (B) combination-treated, (C) erlotinib-treated, and (D) PBS-treated lung adenocarcinomas.

dryer (Labconco FreezeZone 4.6), and lyophilization was performed for 48 hr.

Murine Models of Metastatic NSCLC

Lung cancer models of NSCLC were created by injecting 5×10^6 A549-luciferase cells in sterile PBS into the tail veins of female SCID beige mice. Cancer development and progression were monitored using the Xenogen IVIS (PerkinElmer) bioluminescence imaging system. 100 μL of 30 mg/mL Xenolight Rediject D-Luciferin (PerkinElmer) was injected intraperitoneally into the mice approximately 10 min before the animals were imaged.

Drug Treatment and Tissue Harvesting

Following the establishment of detectable lung tumors (2 weeks from the time of induction), mice were divided into four groups of five animals each. The first group was treated with 20 mg/kg erlotinib daily for 4 weeks by oral gavage (100 μL). The second group was treated with AKSLHNs twice a week for 4 weeks at a dose of 0.3 mg/kg by intraperitoneal injection (100 μL). A third group was treated with a combination of AKSLHNs and erlotinib, whereas the fourth group was treated with PBS as a control twice a week by intraperitoneal injection (100 μL). The animals were monitored weekly with the IVISweekly. The mice were sacrificed 24 hr after the last dose. The lungs were harvested and subdivided into four groups for downstream applications. One part of the tissue was fixed in 10% phosphate-buffered formalin (Fisher Scientific) for paraffin embedding, histology, and immunohistochemistry (IHC) analysis, and other three were snap-frozen for real-time PCR, western blot, and cell death detection ELISA. Tissues snap-frozen in liquid nitrogen were stored at −80°C before analysis.

Evaluation of Immune/Inflammatory Response in Mice

Nine BALB/c wild-type mice were used for this experiment. Five mice were treated with a single dose of 0.9 mg/kg AKSLHNs by intraperitoneal injection, whereas the remaining four served as controls and were injected with PBS (100 μL per mouse). Blood was collected by retro-orbital puncture under isoflurane anesthesia into EDTA-covered Vacutainers (Becton Dickinson) on days 1, 2, 6, and 8. Blood was then immediately centrifuged at 1,000 × *g* for 10 min at 4°C, and serum was collected and frozen at −80°C until ready to be used.

Splenocytes were isolated from mice injected with functionalized nanoparticles and PBS on days 1, 2, 6, and 8. Conditioned medium was collected after 24 hr and frozen at −80°C until ready to be used.

The levels of IL-6 and TNF-α were measured using the respective ELISA kits according to the manufacturers' instructions.

Isolation of Splenocytes from Mice

Spleens of mice injected with AKSLHNs and PBS were collected, placed into a tube with RPMI medium, and kept on ice. The tube was then transferred to the hood, and the spleen was homogenized by two microscope glass slides. The spleen slurry in 10 mL of RPMI medium was transferred to a 70-μm cell strainer (Falcon) and filtered from clumps. The cell suspension was then centrifuged at 400 × *g* for 10 min at 20°C. The cell pellet was resuspended in 3 mL of ammonium-chloride-potassium (ACK) lysis buffer (Gibco) to get rid of red blood cells. The hemolysis was carried out at room temperature with periodic shaking for 5 min, after which the suspension was reconstituted with 10 mL of fresh RPMI medium and centrifuged at 400 × *g* for 5 min at 20°C. The cell pellet was washed with 10 mL of RPMI medium and spun down at 400 × *g* for 5 min. The resulting cell pellet was dissolved in complete RPMI medium (RPMI 1640 medium, 10% FBS, 1× penicillin/streptomycin [Pen/Strep], 10 mM HEPES), 500,000 cells were seeded in triplicate into wells of a 96-well plate. The cells were incubated for 24 hr, and the conditioned medium was collected and frozen until ready to be used for determination of the proinflammatory cytokines TNFα and IL-6.

Western Blot Analysis

Tumor-bearing lungs were collected from mice, snap-frozen in liquid nitrogen, and kept at −80°C until ready to be used. Tissue lysates were prepared in Pierce radioimmunoprecipitation (RIPA) buffer (Thermo Scientific) with addition of Pierce protease inhibitor mini

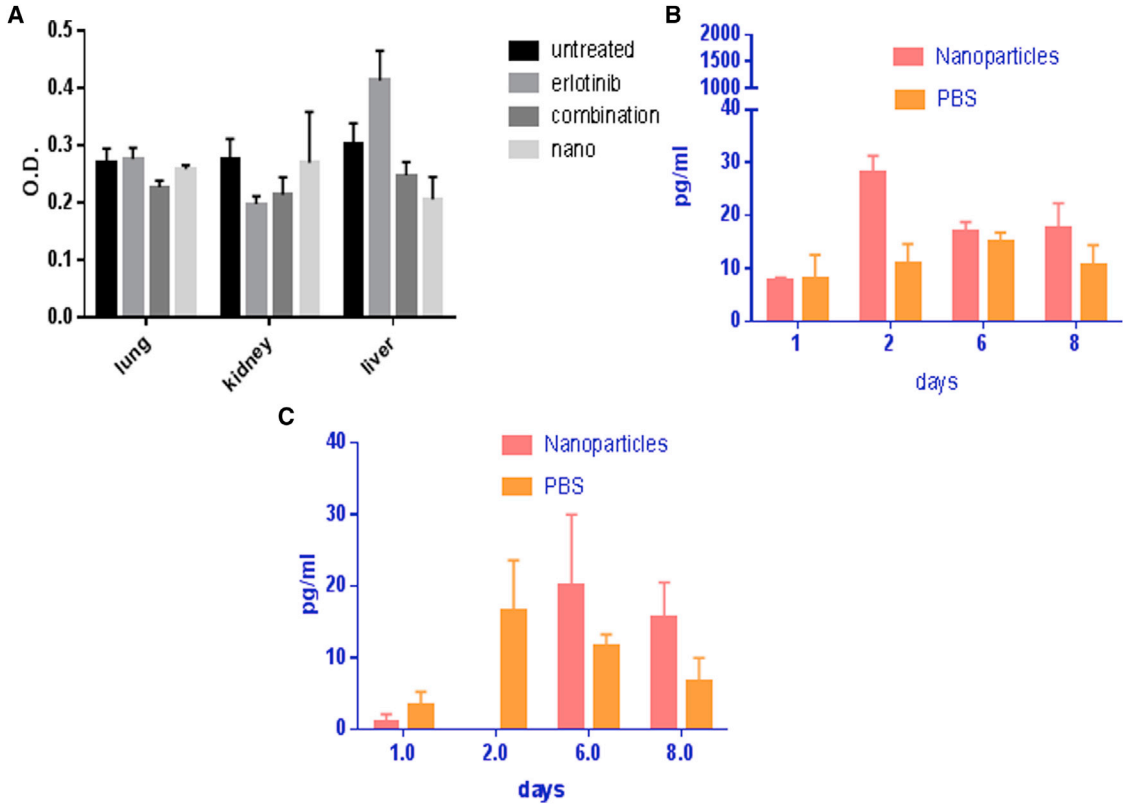

Figure 7. Toxicity to Healthy Tissues and Inflammatory Reaction

(A) Induction of apoptosis in healthy tissues of the lung, kidney, and liver. (B) Expression of IL-6 in splenocytes harvested from the spleens of treated BALB/c mice. (C) Expression of TNF-α in splenocytes harvested from the spleens of treated BALB/c mice (n = 5). Error bars are ± SD.

tablets (Thermo Scientific). The protein concentration was determined with the Coomassie Plus (Bradford) assay kit (Thermo Scientific). 80 μg of total protein was separated on NuPAGE 4%–12% Bis-Tris gels (Life Technologies) with NuPAGE MES SDS running buffer (Life Technologies) and subsequently transferred onto a nitrocellulose membrane of 0.45-μm pore size (Life Technologies). The membrane with proteins was blocked according to the manufacturer's instructions (Invitrogen) for 1 hr at room temperature and probed with primary antibodies—KRAS G12S monoclonal antibody (1:500, New East Biosciences) and β-actin (1:5,000, Sigma-Aldrich)—overnight at 4°C. The membranes were washed three times for 5 min in wash buffer according to the manufacturer's instructions (Invitrogen) and incubated with secondary goat anti-mouse antibodies conjugated with horseradish peroxidase (Molecular Probes) at a dilution of 1:1,000. Immune complexes were detected with chemoluminescent substrate, Pierce ECL western blotting substrate (Thermo Scientific) in a dark room on a tabletop processor, SRX-101A (Konica Minolta). Images were quantified with ImageJ software.

Real-Time TaqMan PCR

Total RNA from snap-frozen lung tissues was isolated with the QIAGEN RNAeasy kit, and cDNA was made with the Verzo cDNA kit (Thermo Scientific) using polyA primers. Real-time PCR was carried out in 20-μL reaction mixtures containing 25 ng of cDNA, 10 μL of 2× TaqMan Gene Expression Master Mix (Applied Biosystems), and 1 μL of specific TaqMan Gene Expression Assay (20×, FAM dye-labeled). Gene expression assays (obtained from Thermo Scientific) contained mutant KRAS at G12S and β-actin primers (β-actin served as a normalizing gene). The corresponding assay numbers were AIX0197 for KRAS G12S and Hs01060665_g1 for β-actin. All samples were run in triplicate.

TUNEL Method for Apoptosis Detection

Apoptosis in samples collected from mice with NSCLC was detected by TUNEL assay with the TACS 2TdT-Fluor in situ apoptosis detection kit (Trevigen) according to the manufacturer's instructions. Briefly, lung tissue section slides were deparaffinized in xylene and 100%, 95%, 70% ethanol, followed by two changes of PBS. Next, the samples were digested with 50 μL of Cytonin solution for 30 min and washed with water and terminal deoxynucleotidyl transferase (TdT) labeling buffer. Next, the slides were covered with 50 μL of labeling reaction mix (TdT deoxynucleoside triphosphate [dNTP], Co^{2+}, TdT enzyme and TdT labeling buffer) and incubated for 60 min at 37°C in a humidity chamber. At this step, negative control was generated by omitting TdT enzyme. Positive control was

made before the labeling step by incubating the slide with TACS nuclease (generating DNA breaks in every cell) at room temperature for 40 min. The labeling reaction was halted by stop buffer, and samples were washed in PBS and covered with 50 μL of strep-fluorescein solution for 20 min. Next, the slides were washed with PBS, mounted, and viewed under a fluorescence microscope with a 495-nm filter.

Cell Death Detection ELISA

Cell death detection ELISA was carried out according to the manufacturer's instructions (Roche). Sandwich ELISA was carried out to determine the amount of mono- and oligonucleosomes in the cytoplasmic fraction of tissue lysates.

Briefly, tissue lysates were prepared as reportedpreviously[32] with some modifications. 2% homogenate of lung tissue was prepared in incubation buffer and centrifuged for 10 min at 15,000 × *g*. The supernatant was collected and kept at −80°C until ready to use.

Plastic wells were incubated with coating solution (containing anti-histone antibodies) overnight at 4°C. The next day, it was substituted for incubation buffer for 30 min and washed three times with washing solution. 100 μL of homogenate, diluted 29 times in incubation buffer, was placed into the wells and kept for 90 min at room temperature with mild shaking. The plate was washed three times and incubated with conjugate solution containing anti-DNA-peroxidase antibodies for 90 min. The wells were washed three times and exposed to ABTS substrate for 30 min until the color developed. Absorption values were read on a BioTek Instruments Epoch microplate spectrophotometer with Gen5 1.10 software.

Histology

The tissue samples were processed and embedded in paraffin. 4-μm paraffin sections were made for further analysis. Paraffin slides were routinely stained with H&E.

For IHC, the paraffin slides were deparaffinized and rehydrated. Heat-mediated antigen retrieval was performed in citrate buffer (pH 6.0) at 98°C for 20 min. Primary antibody, cleaved caspase-3(catalog no. 9664, Cell Signaling Technology), was diluted 1:300 and incubated at room temperature for 30 min; human tonsil was used as a positive control. Normal rabbit IgG was added as a negative control. The IHC procedure was done with the Dako Autostainer Plus platform using the Vectastain Elite ABC kit (Standard, catalog no. PK-6100, Vector Laboratories) according to the manufacturer's instructions. DAB substrate (catalog no. k34568, Dako) was used for visualization.

Statistical Analysis

Results are presented as mean ± SD unless otherwise indicated. Statistically significant differences between two groups were determined by two-tailed Student's t test. A p value of 0.05 was taken as statistically significant.

SUPPLEMENTAL INFORMATION

Supplemental Information includes three figures and can be found with this article online at http://dx.doi.org/10.1016/j.omtn.2016.12.009.

AUTHOR CONTRIBUTIONS

M.P. carried out most of the experiments and was also involved in data interpretation. O.S. and R.B. were involved in taking pictures of the histology slides and the interpretation of histopathology data. C.T., Y.L., R.B.D., A.E.S., and B.L. were involved in the development and monitoring of the orthotopic metastatic mouse lung cancer models. S.A.S. initiated the study, planned the experiments, interpreted the data, and wrote the manuscript.

CONFLICTS OF INTEREST

The authors declare no conflict of interest.

ACKNOWLEDGMENTS

We acknowledge the support of the Science Center, Philadelphia, and Thomas Jefferson University of this project through the award of QED Grant S1402.

REFERENCES

1. Jemal, A., Siegel, R., Ward, E., Murray, T., Xu, J., and Thun, M.J. (2007). Cancer statistics CA. Cancer J. Clin *57*, 43–66.
2. Greenlee, R.T., Murray, T., Bolden, S., and Wingo, P.A. (2000). Cancer statistics, 2000. CA Cancer J. Clin. *50*, 7–33.
3. Zalipsky, S., Saad, M., Kiwan, R., Ber, E., Yu, N., and Minko, T. (2007). Antitumor activity of new liposomal prodrug of mitomycin C in multidrug resistant solid tumor: insights of the mechanism of action. J. Drug Target. *15*, 518–530.
4. Garbuzenko, O.B., Saad, M., Pozharov, V.P., Reuhl, K.R., Mainelis, G., and Minko, T. (2010). Inhibition of lung tumor growth by complex pulmonary delivery of drugs with oligonucleotides as suppressors of cellular resistance. Proc. Natl. Acad. Sci. USA *107*, 10737–10742.
5. Gottesman, M.M. (2002). Mechanisms of cancer drug resistance. Annu. Rev. Med. *53*, 615–627.
6. Fukuoka, M., Yano, S., Giaccone, G., Tamura, T., Nakagawa, K., Douillard, J.Y., Nishiwaki, Y., Vansteenkiste, J., Kudoh, S., Rischin, D., et al. (2003). Multi-institutional randomized phase II trial of gefitinib for previously treated patients with advanced non-small-cell lung cancer (The IDEAL 1 Trial) [corrected]. J. Clin. Oncol. *21*, 2237–2246.
7. Kris, M.G., Natale, R.B., Herbst, R.S., Lynch, T.J., Jr., Prager, D., Belani, C.P., Schiller, J.H., Kelly, K., Spiridonidis, H., Sandler, A., et al. (2003). Efficacy of gefitinib, an inhibitor of the epidermal growth factor receptor tyrosine kinase, in symptomatic patients with non-small cell lung cancer: a randomized trial. JAMA *290*, 2149–2158.
8. Pérez-Soler, R., Chachoua, A., Hammond, L.A., Rowinsky, E.K., Huberman, M., Karp, D., Rigas, J., Clark, G.M., Santabárbara, P., and Bonomi, P. (2004). Determinants of tumor response and survival with erlotinib in patients with non–small-cell lung cancer. J. Clin. Oncol. *22*, 3238–3247.
9. Pao, W., Wang, T.Y., Riely, G.J., Miller, V.A., Pan, Q., Ladanyi, M., Zakowski, M.F., Heelan, R.T., Kris, M.G., and Varmus, H.E. (2005). KRAS mutations and primary resistance of lung adenocarcinomas to gefitinib or erlotinib. PLoS Med. *2*, e17.
10. Tam, I.Y., Chung, L.P., Suen, W.S., Wang, E., Wong, M.C., Ho, K.K., Lam, W.K., Chiu, S.W., Girard, L., Minna, J.D., et al. (2006). Distinct epidermal growth factor receptor and KRAS mutation patterns in non-small cell lung cancer patients with different tobacco exposure and clinicopathologic features. Clin. Cancer Res. *12*, 1647–1653.
11. Eberhard, D.A., Johnson, B.E., Amler, L.C., Goddard, A.D., Heldens, S.L., Herbst, R.S., Ince, W.L., Jänne, P.A., Januario, T., Johnson, D.H., et al. (2005). Mutations

in the epidermal growth factor receptor and in KRAS are predictive and prognostic indicators in patients with non-small-cell lung cancer treated with chemotherapy alone and in combination with erlotinib. J. Clin. Oncol. *23*, 5900–5909.

12. Tsao, M., Zhu, C., Sakurada, A., Zhang, T., Whitehead, M., Kamel-Reid, S., Ding, K., Seymour, L., and Shepherd, F. (2006). An analysis of the prognostic and predictive importance of K-ras mutation status in the National Cancer Institute of Canada Clinical Trials Group BR.21 study of erlotinib versus placebo in the treatment of non-small cell lung cancer. J. Clin. Oncol. *24* (18_suppl), 7005.
13. Miller, V.A., Zakowski, M., Riely, G.J., Pao, W., Ladanyi, M., Tsao, A.S., Sandler, A., Herbst, R., Kris, M.G., and Johnson, D.H. (2006). EGFR mutation and copy number, EGFR protein expression and KRAS mutation as predictors of outcome with erlotinib in bronchioloalveolar cell carcinoma (BAC): Results of a prospective phase II trial. J. Clin. Oncol. *24* (18_suppl), 7003.
14. Pao, W., Miller, V., Zakowski, M., Doherty, J., Politi, K., Sarkaria, I., Singh, B., Heelan, R., Rusch, V., Fulton, L., et al. (2004). EGF receptor gene mutations are common in lung cancers from "never smokers" and are associated with sensitivity of tumors to gefitinib and erlotinib. Proc. Natl. Acad. Sci. USA *101*, 13306–13311.
15. Jagani, H.V., Josyula, V.R., Hariharapura, R.C., Palanimuthu, V.R., and Gang, S.S. (2011). Nanoformulation of siRNA silencing Bcl-2 gene and its implication in cancer therapy. Arzneimittelforschung *61*, 577–586.
16. Kim, V.N. (2003). RNA interference in functional genomics and medicine. J. Korean Med. Sci. *18*, 309–318.
17. Shim, M.S., and Kwon, Y.J. (2010). Efficient and targeted delivery of siRNA in vivo. FEBS J. *277*, 4814–4827.
18. de Fougerolles, A., Vornlocher, H.P., Maraganore, J., and Lieberman, J. (2007). Interfering with disease: a progress report on siRNA-based therapeutics. Nat. Rev. Drug Discov. *6*, 443–453.
19. Kalluri, J.R., Arbneshi, T., Khan, S.A., Neely, A., Candice, P., Varisli, B., Washington, M., McAfee, S., Robinson, B., Banerjee, S., et al. (2009). Use of gold nanoparticles in a simple colorimetric and ultrasensitive dynamic light scattering assay: selective detection of arsenic in groundwater. Angew. Chem. Int. Ed. Engl. *48*, 9668–9671.
20. Xue, H.Y., and Wong, H.L. (2011). Solid lipid-PEI hybrid nanocarrier: an integrated approach to provide extended, targeted, and safer siRNA therapy of prostate cancer in an all-in-one manner. ACS Nano *5*, 7034–7047.
21. Lakshmikuttyamma, A., Sun, Y., Lu, B., Undieh, A.S., and Shoyele, S.A. (2014). Stable and efficient transfection of siRNA for mutated KRAS silencing using novel hybrid nanoparticles. Mol. Pharm. *11*, 4415–4424.
22. Perepelyuk, M., Thangavel, C., Liu, Y., Den, R.B., Lu, B., Snook, A.E., and Shoyele, S.A. (2016). Biodistribution and Pharmacokinetic study of siRNA-loaded anti-NTSR1-mAb-functionalized novel hybrid nanoparticles in metastatic orthotopic murine lung cancer model. Mol. Ther. Nucleic Acids *5*, e282.
23. Dim, N., Perepelyuk, M., Gomes, O., Thangavel, C., Liu, Y., Den, R., Lakshmikuttyamma, A., and Shoyele, S.A. (2015). Novel targeted siRNA-loaded hybrid nanoparticles: preparation, characterization and in vitro evaluation. J. Nanobiotechnology *13*, 61.
24. Yousefpour, P., Atyabi, F., Vasheghani-Farahani, E., Movahedi, A.A., and Dinarvand, R. (2011). Targeted delivery of doxorubicin-utilizing chitosan nanoparticles surface-functionalized with anti-Her2 trastuzumab. Int. J. Nanomedicine *6*, 1977–1990.
25. Xiong, L., Shuhendler, A.J., and Rao, J. (2012). Self-luminescing BRET-FRET near-infrared dots for in vivo lymph-node mapping and tumour imaging. Nat. Commun. *3*, 1193.
26. Linardou, H., Dahabreh, I.J., Kanaloupiti, D., Siannis, F., Bafaloukos, D., Kosmidis, P., Papadimitriou, C.A., and Murray, S. (2008). Assessment of somatic k-RAS mutations as a mechanism associated with resistance to EGFR-targeted agents: a systematic review and meta-analysis of studies in advanced non-small-cell lung cancer and metastatic colorectal cancer. Lancet Oncol. *9*, 962–972.
27. Sunaga, N., Shames, D.S., Girard, L., Peyton, M., Larsen, J.E., Imai, H., Soh, J., Sato, M., Yanagitani, N., Kaira, K., et al. (2011). Knockdown of oncogenic KRAS in non-small cell lung cancers suppresses tumor growth and sensitizes tumor cells to targeted therapy. Mol. Cancer Ther. *10*, 336–346.
28. Srinivasan, A.R., and Shoyele, S.A. (2014). Influence of Surface Modification and the pH on the Release Mechanisms and Kinetics of Erlotinib from Antibody-Functionalized Chitosan Nanoparticles. Ind. Eng. Chem. Res. *53*, 2987–2993.
29. Sahay, G., Querbes, W., Alabi, C., Eltoukhy, A., Sarkar, S., Zurenko, C., Karagiannis, E., Love, K., Chen, D., Zoncu, R., et al. (2013). Efficiency of siRNA delivery by lipid nanoparticles is limited by endocytic recycling. Nat. Biotechnol. *31*, 653–658.
30. Jagani, H.V., Josyula, V.R., Palanimuthu, V.R., Hariharapura, R.C., and Gang, S.S. (2013). Improvement of therapeutic efficacy of PLGA nanoformulation of siRNA targeting anti-apoptotic Bcl-2 through chitosan coating. Eur. J. Pharm. Sci. *48*, 611–618.
31. Aigner, A. (2007). Applications of RNA interference: current state and prospects for siRNA-based strategies in vivo. Appl. Microbiol. Biotechnol. *76*, 9–21.
32. Arora, A.K. (2011). Erlotinib-induced hepatotoxicity-Clinical presentation and successful management: A case report. J. Clin. Exp. Hepatol. *1*, 38–40.

OMTN, Volume *6*

Supplemental Information

siRNA-Encapsulated Hybrid Nanoparticles Target Mutant K-*ras* and Inhibit Metastatic Tumor Burden in a Mouse Model of Lung Cancer

Maryna Perepelyuk, Olubunmi Shoyele, Ruth Birbe, Chellappagounder Thangavel, Yi Liu, Robert B. Den, Adam E. Snook, Bo Lu, and Sunday A. Shoyele

Supplementary Materials

Supplementary figures

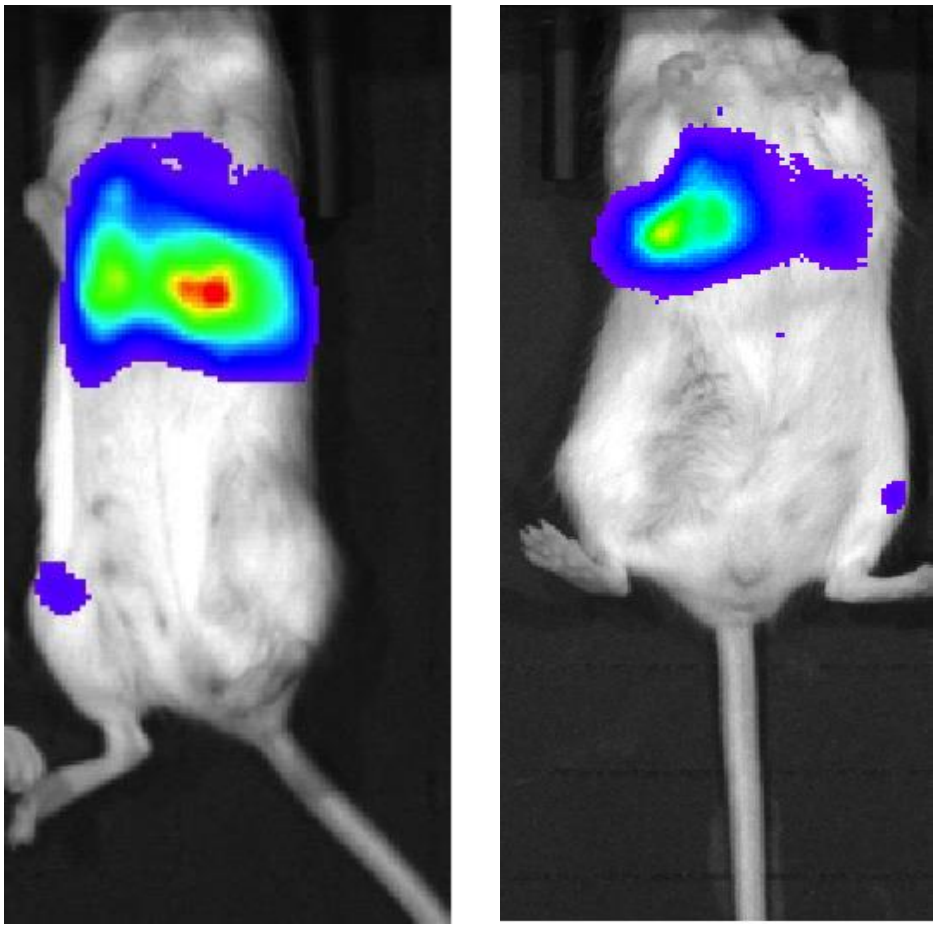

Fig. S1. PBS-treated mice showing tumor metastasis to either the right or left popliteal lymph nodes.

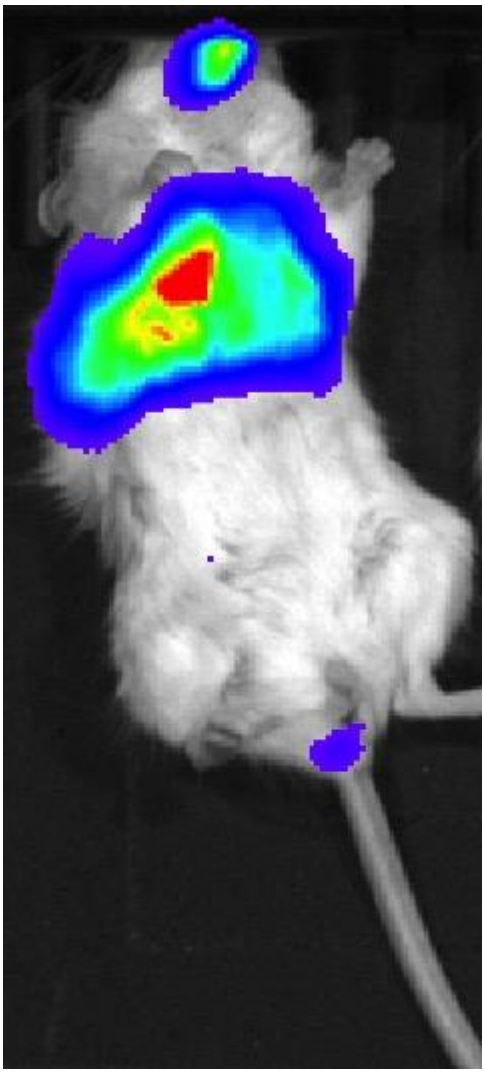

Fig. S2. A mice in the erlotinib treated group showing tumor metastasis in the brain after 4 weeks of treatment.

a

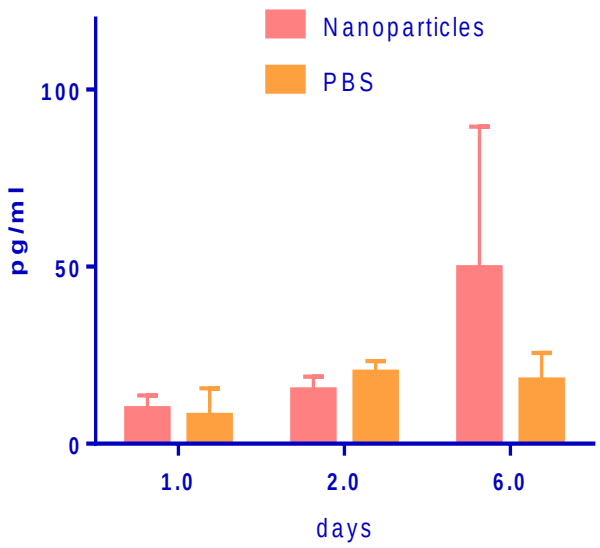

b

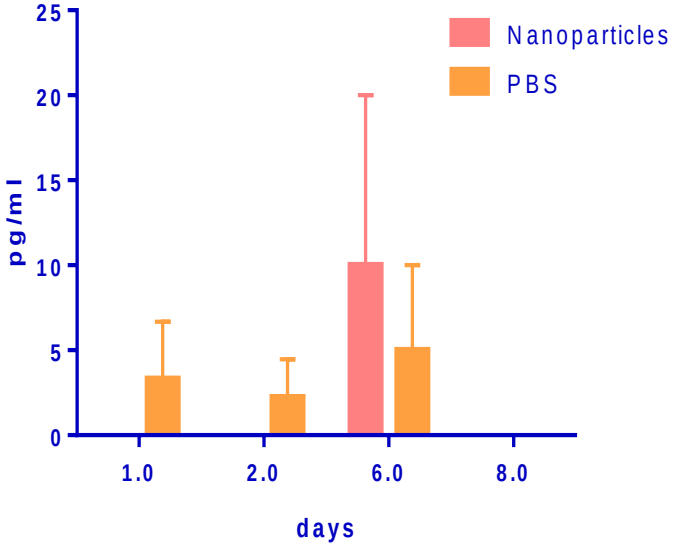

Fig. S3. Cytokine expression in the serum of treated BALB/c mice. a. IL-6 expression. b. TNF-α expression.